AGU ADVANCING EARTH AND SPACE SCIENCE

Geophysical Research Letters

RESEARCH LETTER
10.1029/2022GL100971

Magnetosonic Waves Above the Lower Hybrid Frequency in Cyclotron Resonance With the Van Allen Radiation Belt Electrons

Zhiyong Wu[1,2,3], Zhenpeng Su[1,2,3], Zhaoguo He[4,5,6], Huinan Zheng[1,2,3], and Yuming Wang[1,2,3]

[1]Deep Space Exploration Laboratory/School of Earth and Space Sciences, University of Science and Technology of China, Hefei, China, [2]CAS Center for Excellence in Comparative Planetology/CAS Key Laboratory of Geospace Environment/Mengcheng National Geophysical Observatory, University of Science and Technology of China, Hefei, China, [3]Collaborative Innovation Center of Astronautical Science and Technology, Hefei, China, [4]School of Atmospheric Science, Sun Yat-sen University, Zhuhai, China, [5]School of Atmospheric Sciences, Planetary Environmental and Astrobiological Research Laboratory (PEARL), Sun Yat-sen University, Zhuhai, China, [6]Key Laboratory of Tropical Atmosphere-Ocean System, Sun Yat-sen University, Ministry of Education, Zhuhai, China

Abstract Cyclotron resonance with magnetosonic waves was usually considered unimportant for the Van Allen radiation belt electron dynamics because it occurs at energies that are too high. Here, we show that for magnetosonic waves with frequencies above the lower hybrid frequency and normal angles below 87° in the high-density plasmasphere, the electron cyclotron resonances of ±1, ±2, and ±3 orders can extend down to energies of 10–100s keV. These high-frequency, non-quasi-perpendicular magnetosonic waves are found to occur predominantly in the duskside outer plasmasphere, with an amplitude on the order of 10 pT following strong substorms. They probably originate from midlatitudes of the outer plasmasphere, different from the commonly known magnetosonic waves generated near the equator.

Plain Language Summary Earth's outer radiation belt is composed of electrons with energies from hundreds of keV to several MeV. How electrons are accelerated to high energy and scattered in pitch-angle are two fundamental questions in the radiation belt dynamics. For commonly existing magnetosonic waves, Landau resonance, bounce resonance, and transit-time scattering have been well established as candidate mechanisms. However, electron cyclotron resonance with magnetosonic waves was usually considered unimportant because it occurs at energies that are too high. Here, we show that the electron cyclotron resonant energy can extend down to 10–100s keV for magnetosonic waves with frequencies high enough and normal angles off-90° enough. These high-frequency, non-quasi-perpendicular magnetosonic waves are statistically found to gather in the duskside outer plasmasphere, with an amplitude on the order of 10 pT following strong substorms. Their source region is probably located at midlatitudes of the outer plasmasphere, different from the normal magnetosonic waves generated near the equator. Future works may need to quantify the contribution of these magnetosonic waves to the radiation belt electron dynamics via the fundamental and harmonic cyclotron resonances.

Key Points:

- Electron cyclotron resonance can extend to 10–100s keV for the high-frequency, non-quasi-perpendicular, plasmaspheric magnetosonic waves
- The $f > f_{lh}$ magnetosonic waves occur mainly in the duskside outer plasmasphere, with an average amplitude of 10 pT following strong substorms
- The $f > f_{lh}$ magnetosonic waves are probably generated by the proton Bernstein-mode instability at midlatitudes in the outer plasmasphere

Supporting Information:

Supporting Information may be found in the online version of this article.

Correspondence to:

Z. Su and Z. He,
szpe@mail.ustc.edu.cn;
hezhg3@mail.sysu.edu.cn

Citation:

Wu, Z., Su, Z., He, Z., Zheng, H., & Wang, Y. (2022). Magnetosonic waves above the lower hybrid frequency in cyclotron resonance with the Van Allen radiation belt electrons. *Geophysical Research Letters*, *49*, e2022GL100971. https://doi.org/10.1029/2022GL100971

Received 23 AUG 2022
Accepted 21 NOV 2022

1. Introduction

Magnetosonic waves from the ion Bernstein-mode instability commonly exist in the Earth's inner magnetosphere (Balikhin et al., 2015; Gurnett, 1976; Meredith et al., 2008; Russell et al., 1970). They are usually characterized as highly oblique, compressional, electromagnetic waves in the frequency range from several hertz to hundreds of hertz (Boardsen et al., 2018; Russell et al., 1970; Santolík et al., 2004; Su et al., 2017; X. Yu et al., 2021). These magnetosonic waves have been proposed to accelerate or scatter the Van Allen radiation belt electrons through Landau resonance (Fu et al., 2019; Horne et al., 2007; J. Li et al., 2016; L. Y. Li et al., 2017; Xiao et al., 2015), transit-time scattering (Bortnik & Thorne, 2010; Bortnik et al., 2015; J. Li et al., 2014; J. Yu et al., 2019; X. Yu et al., 2020), and bounce resonance (Chen et al., 2015; Maldonado & Chen, 2018; Shprits, 2016; Tao & Li, 2016). Under the assumption of quasi-perpendicular propagation, the magnetosonic waves are in cyclotron resonance with electrons above several MeV (Horne et al., 2007). Therefore, the cyclotron resonances of magnetosonic waves are usually considered to be unimportant for the radiation belt electron dynamics (Horne et al., 2007).

Recently, magnetosonic waves have been found to occur far away from the magnetic equator (Boardsen et al., 2016; Ni et al., 2018; Tsurutani et al., 2014; Yuan et al., 2019; Zhima et al., 2015) or above the lower hybrid

frequency f_{lh} (Boardsen et al., 2016; Wu et al., 2021). According to the ray-tracing simulations, when magnetosonic waves propagate from the midlatitudes to the equator, their normal angles deviate significantly from 90° (Boardsen et al., 1992, 2016; Wu et al., 2021; Zhima et al., 2015). Boardsen et al. (2016) first mentioned the presence of magnetosonic waves above the lower hybrid frequency. These high-frequency, magnetosonic waves were further explained as a result of the proton Bernstein-mode instability at midlatitudes inside the plasmasphere (Wu et al., 2021). According to the cold plasma wave dispersion relation, the normal angles of magnetosonic waves above f_{lh} have to fall away from 90° (Stix, 1962; Wu et al., 2021). These findings inspire us to reexamine the possibility of these high-frequency, non-quasi-perpendicular magnetosonic waves to cyclotron resonate with the radiation belt electrons over a broad range of energies.

2. Minimum Landau and Cyclotron Resonant Energies

The Landau and cyclotron resonance condition is given by

$$\omega - k_{\parallel} v_{\parallel} = -n \left|\Omega_{ce}\right| / \gamma, \tag{1}$$

with the wave angular frequency $\omega = 2\pi f$, the parallel wavevector $k_{\parallel} = k\cos\psi$, the wave normal angle ψ, the electron angular gyro-frequency $|\Omega_{ce}| = 2\pi f_{ce}$, the electron parallel velocity $v_{\parallel} = v\cos\alpha$, the electron pitch-angle α, the Lorentz factor $\gamma = 1/\sqrt{1 - v^2/c^2}$, and the resonance order n ($n = 0$ for the Landau resonance and $n = \pm 1$, ± 2, ± 3, $\cdots$ for the cyclotron resonances). In velocity space with parallel velocity $v_{\parallel}$ as the horizontal axis and perpendicular velocity $v_{\perp}$ as the vertical axis, the Landau resonance condition for a fixed wave follows a vertical line $v_{\parallel} = \omega/k_{\parallel}$ and the cyclotron resonance condition follows an ellipse $v_{\parallel}^2 + v_{\perp}^2 + \left(\frac{k_{\parallel} c}{n\Omega_e}\right)^2 \left(v_{\parallel} - \frac{\omega}{k_{\parallel}}\right)^2 = c^2$ (Horne & Thorne, 1998; Summers et al., 1998). Both Landau and cyclotron resonant electrons have the minimum energy E_{min} at $v_{\perp} = 0$ (Horne et al., 2000; Horne & Thorne, 1998; Summers et al., 1998, 2007). When $\omega \ll n\left|\Omega_{ce}\right| / \gamma$, the minimum resonant energy E_{min} is approximately independent of the sign of the resonance order n.

Figure 1 shows the dependence of the minimum resonant energy E_{min} on the wave frequency f/f_{ce} and normal angle ψ. Because of the density-dependence of $k_{\parallel}$, E_{min} inside the plasmasphere ($f_{pe}/f_{ce} = 20$) is approximately 1 order of magnitude lower than that outside the plasmasphere ($f_{pe}/f_{ce} = 5$). (Note that f_{pe} is the electron plasma frequency.) Both inside and outside the plasmasphere, $E_{min}^{n\neq 0}$ is more than 3 orders of magnitude higher than $E_{min}^{n=0}$. With the increase of f/f_{ce}, the decrease of ψ, and the decrease of n, $E_{min}^{n\neq 0}$ rapidly decreases. Particularly, when $f > f_{lh}$ and $\psi < 87°$, $E_{min}^{n\neq 0}$ falls to 10–100 keV inside the plasmasphere. These calculations imply that the high-frequency and non-quasi-perpendicular magnetosonic waves could contribute to the radiation belt electron dynamics through the cyclotron resonances. Questions arise as to when, where, and how these magnetosonic waves could occur.

3. Spatiotemporal Distribution of $f > f_{lh}$ Magnetosonic Waves

In contrast to previous statistical studies of magnetosonic waves below f_{lh} (Ma et al., 2013, 2019; Meredith et al., 2008; Němec et al., 2013; Santolík et al., 2004; Teng et al., 2019; Tsurutani et al., 2014; Yan et al., 2021), we focus on the spatiotemporal distribution of magnetosonic waves above f_{lh}. The ambient electron density (Kurth et al., 2015), magnetic field strength, and wave electromagnetic spectral matrix were acquired by the Electric and Magnetic Field Instrument Suite and Integrated Science (EMFISIS; Kletzing et al., 2013) suite onboard the Van Allen Probes mission (Mauk et al., 2013) from November 2012 to July 2019. The wave normal angle, ellipticity and planarity are determined by the singular value decomposition technique (Santolík et al., 2003). First, waves with sufficiently strong power spectral densities $P_B > 10^{-8}$ nT^{2}Hz^{-1}, large normal angles $\psi > 75°$, and high planarities $F_B > 0.7$ are identified as candidate magnetosonic waves. These criteria are comparable to those used in previous magnetosonic wave statistics (Ma et al., 2019; Teng et al., 2019; Yan et al., 2021). Next, the candidate waves significantly deviating from the theoretical predictions are removed. Cold plasma wave theory predicts a reasonable range of the ratio between magnetic and electric power spectral densities $\left[\min\left\{\frac{P_B(\psi)}{P_E(\psi)}\right\}, \max\left\{\frac{P_B(\psi)}{P_E(\psi)}\right\}\right]$ with normal angles $75° \le \psi \le 90°$. A candidate wave with the ratio falling outside this range is removed. This procedure can largely suppress contamination from background noise. Finally, the highly sparse candidate waves are removed. Specifically, if a candidate wave is the only element in a 3×3 time-frequency matrix centering at it, this candidate wave is identified as a sparse candidate wave. The wave occurrence location with respect to the plasmapause is identified automatically according to the electron density threshold proposed by W.

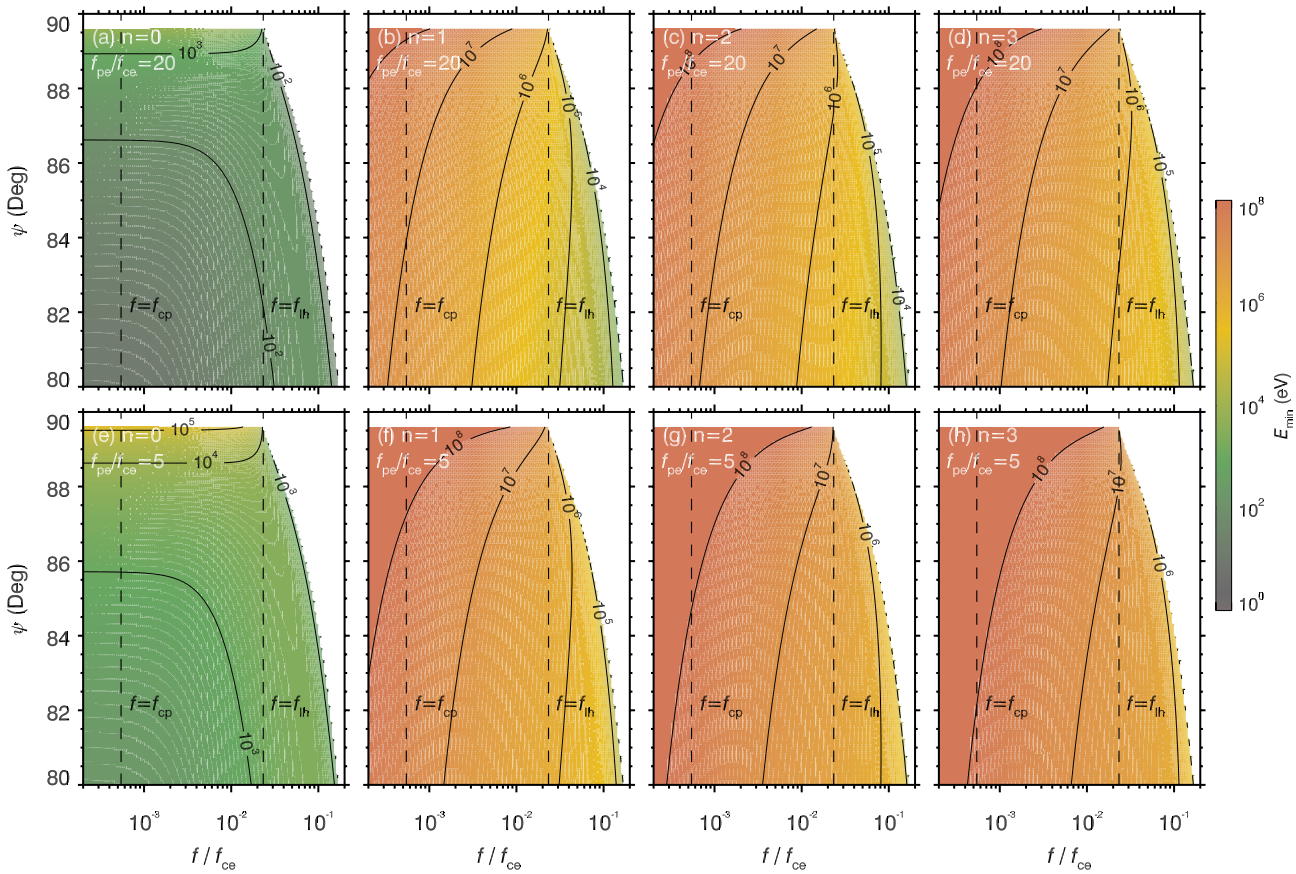

Figure 1. Minimum resonant energy for electrons (a–d) inside (f_{pe}/f_{ce} = 20) and (e–h) outside (f_{pe}/f_{ce} = 5) the plasmasphere at the different resonance orders (indicated). Vertical dashed lines mark the proton cyclotron frequency f_{cp} and the lower hybrid frequency f_{lh}.

Li et al. (2010) and then amended artificially according to the spatial distribution of plasmaspheric hiss. A candidate wave is identified to be inside the plasmasphere, if its corresponding density exceeds a critical value $N_c = \max\left\{10 \times \left(\frac{6.6}{L}\right)^4, 50\right\}$ cm^{-3} (Moldwin et al., 1994; Sheeley et al., 2001). When the density profile has a clear jump at the plasmapause, this procedure is effective; in contrast, it becomes ambiguous when the density profile is extending smoothly outward. For the latter case, the candidate magnetosonic waves accompanied by whistler-mode hiss waves are artificially identified to be inside the plasmasphere. In Figure S1, we show two representative $f > f_{lh}$ magnetosonic wave events inside and outside the plasmasphere.

Figure 2 shows the root-mean-square (RMS) amplitude $\langle B_W \rangle$ as a function of magnetic shell L and magnetic local time MLT inside and outside the plasmasphere under different levels of substorm activities. The cumulative impact of substorm activities on the magnetosonic waves is measured by SME*, the maximum SuperMAG electrojet (SME) index (Newell & Gjerloev, 2011) within the preceding 3 hr. To ensure statistical soundness as much as possible, we have omitted the bins with <10 samples from the calculation of $\langle B_W \rangle$. Such bins mainly occur during weak substorms (SME* < 400 nT). In the bins with ≥10 samples, 60% of the samples have amplitudes >5 pT. Contrary to the preferential occurrence of the $f < f_{lh}$ magnetosonic waves outside the plasmasphere (B. Liu et al., 2018; Ma et al., 2014; Posch et al., 2015), the $f > f_{lh}$ magnetosonic waves predominantly occur inside the duskside (15 < MLT < 21) outer plasmasphere (5 < L < 6). There are approximately 1 order of magnitude more wave samples inside than outside the plasmasphere. As the substorm intensity increases, the wave amplitude increases, and the occurrence region expands. Following strong substorms (SME* > 400 nT), all of the L-MLT bins with wave amplitudes of 10–30 pT are inside the plasmasphere. The average amplitude of the $f > f_{lh}$ magnetosonic waves is approximately five times smaller than that of the $f < f_{lh}$ magnetosonic waves (Kim & Shprits, 2018;

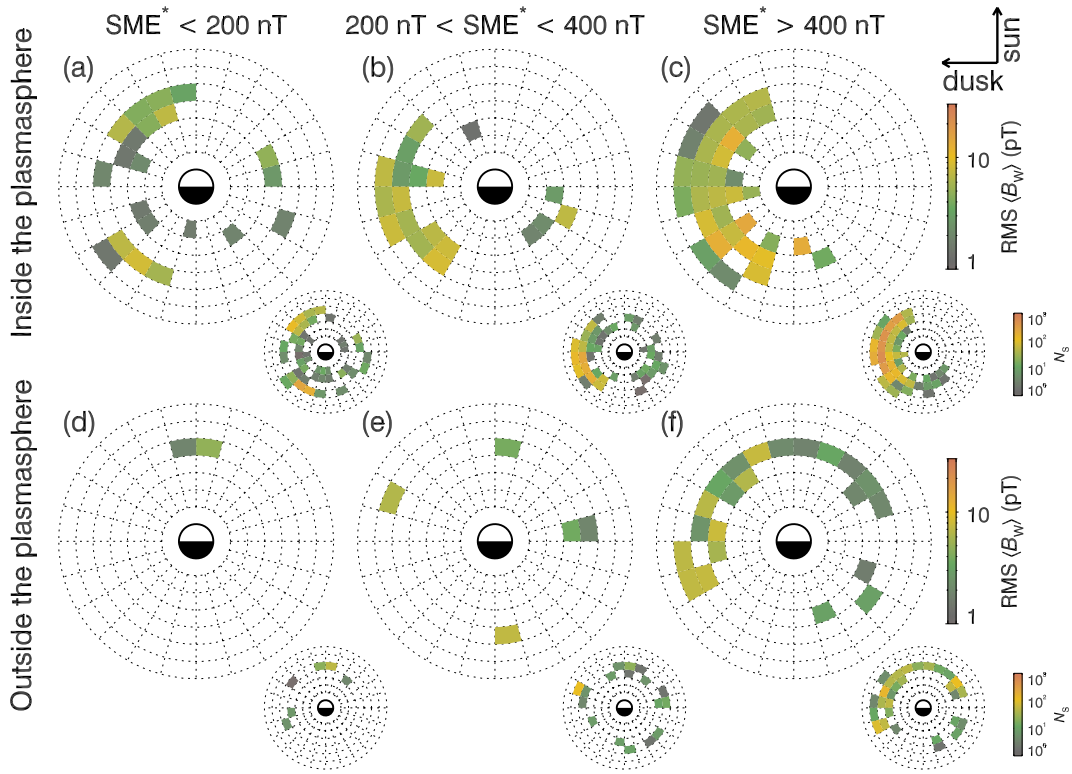

Figure 2. Global L–MLT maps of the root-mean-square amplitude $\langle B_W \rangle$ (main panels) and the sample numbers N_S (subpanels) of the $f > f_{lh}$ magnetosonic waves inside and outside the plasmasphere under increasing substorm activities (from left to right). Bins with <10 samples are omitted from the calculation of $\langle B_W \rangle$ in the main panels.

Ma et al., 2019; Teng et al., 2019; Yan et al., 2021). The SME*-dependence and MLT-dependence of magnetosonic waves imply that they could be generated by westward drifting protons injected during substorms.

Figure 3 presents the wave normal angle and frequency distributions of the $f > f_{lh}$ magnetosonic waves in the duskside ($15 < \text{MLT} < 21$) plasmasphere. The number of these wave samples peaks at $5 < L < 6$ and decreases toward two sides. Because of the Van Allen Probes mission's low orbital inclination (Mauk et al., 2013), fewer wave samples are farther from the equator. Similar to Figure 2, we have omitted the bins with <10 samples from the calculation of median power-weighted wave normal angles $\langle \psi \rangle$. Within $4 < L < 7$, $\langle \psi \rangle$ increases systematically from 83.5° to 85.5° from the equator to the farthest magnetic latitude (MLAT = ±20°). As discussed by Boardsen et al. (2016), the wave normal angle values derived from the spectral matrix have an uncertainty of approximately 3°. Therefore, one should be cautious about these quantitative data of $\langle \psi \rangle$. Nevertheless, given that the proton Bernstein-mode instability mainly arises at the quasi-perpendicular direction (Chen, 2015), the qualitative trend of $\langle \psi \rangle$ supports the off-equatorial generation scenario (Wu et al., 2021). These waves mainly occur below $2.5f_{lh}$ and occasionally extend to $3.3f_{lh}$. The bins above $2.5f_{lh}$ have <10 samples, which have been omitted from the calculation of median magnetic power spectral density $\langle P_B \rangle$. $\langle P_B \rangle$ systematically decreases with increasing frequency. These wave normal angle and frequency characteristics are qualitatively consistent with the prediction of cold plasma wave theory. As indicated in Figure 1, these high-frequency, non-quasi-perpendicular magnetosonic waves could contribute to the dynamics of radiation belt electrons above 10–100s keV through the $n = \pm 1, \pm 2$, and ± 3 cyclotron resonances.

4. Generation of $f > f_{lh}$ Magnetosonic Waves

To understand the generation of these $f > f_{lh}$ magnetosonic waves, we use the previously developed code (N. Liu et al., 2018a, 2018b; Su et al., 2018) to quantify the latitude-dependent Bernstein-mode instability of energetic protons (Figure 4). We have analyzed energetic proton measurements by the Helium Oxygen Proton Electron Mass Spectrometer (HOPE; Funsten et al., 2013) of the Energetic particle, Composition and the Thermal

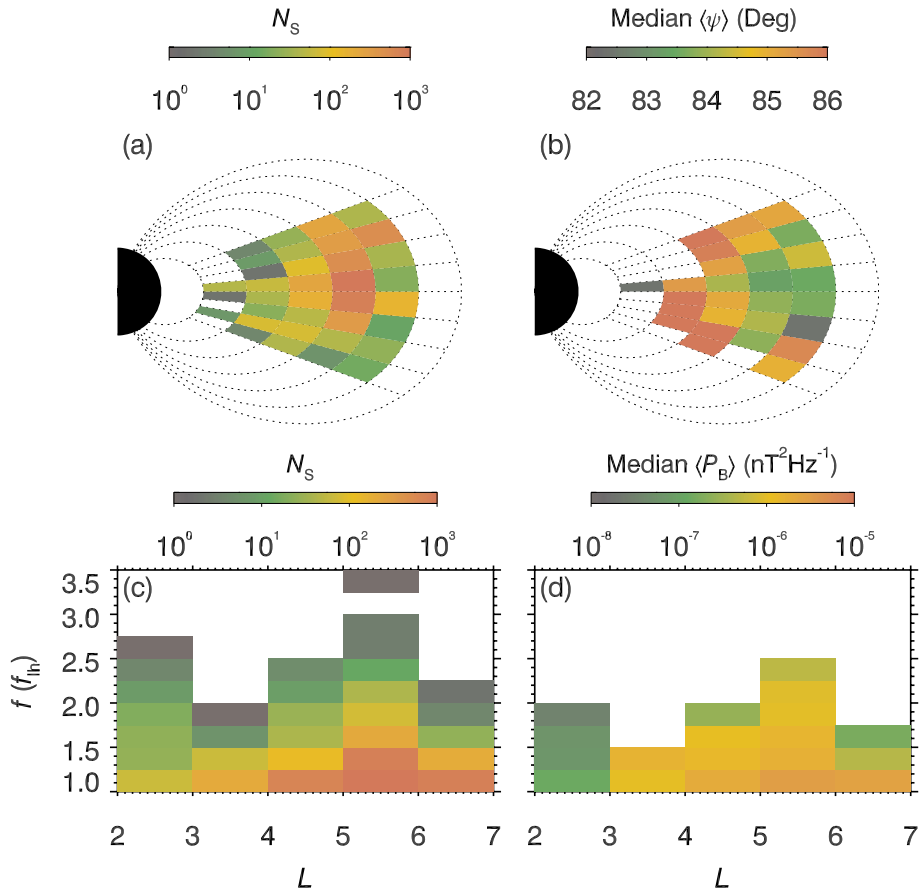

Figure 3. Global L–MLAT and $L-f$ maps of (a) and (c) the sample number N_S, (b) the median power-weighted wave normal angle $\langle\psi\rangle$, and (d) the median magnetic power spectral density $\langle P_B\rangle$ of the $f > f_{lh}$ magnetosonic waves in the duskside (15 < MLT < 21) plasmasphere. Bins with <10 samples are omitted from the calculations of $\langle\psi\rangle$ and $\langle P_B\rangle$ in (b and d).

plasma suite (ECT; Spence et al., 2013) onboard the Van Allen Probes mission for all the $f > f_{lh}$ magnetosonic wave events in the duskside (15 < MLT < 21) outer plasmasphere (5.35 < L < 5.65). In each latitudinal bin with measurements available (Figures 4a–4d), we assume the proton phase space density in the form of $F(\alpha,\ E_k,\ \text{MLAT}) = F_\perp(E_k,\ \text{MLAT}) \cdot \overline{F}(\alpha)$ (Figures 4e–4h), where the perpendicular phase space density $F_\perp(E_k,\ \text{MLAT})$ is chosen as the energy-dependent median profile and the pitch-angle dependence is approximated as $\overline{F}(\alpha) = \left(\frac{1+\sin\alpha}{2}\right)^2$. According to Liouville's theorem, the modeled profile in the 15°–20° latitudinal bin is further mapped to higher latitudes without measurements (Figure 4i). To fit the latitudinal measurements of magnetic fields, we adopt an analytical geomagnetic field model of Kabin et al. (2007) in a spherical coordinate system (r, θ, ϕ)

$$\mathbf{B} = -\mathbf{e}_r\left[2B_E\left(\frac{R_E}{r}\right)^3 - B_{RC}\right]\cos\theta - \mathbf{e}_\theta\left[B_E\left(\frac{R_E}{r}\right)^3 + B_{RC}\right]\sin\theta, \tag{2}$$

with $B_E = 31{,}200$ nT and $B_{RC} = -50$ nT related to the Earth's intrinsic dipole and the enhanced partial ring current (Figure 4j). Following the previous work of Denton et al. (2002), we fit the latitude-dependent electron density in the form of

$$N_e\,(\text{MLAT}) = N_{eq}\cos^{-2\nu}(\text{MLAT}), \tag{3}$$

with the equatorial density $N_{eq} = 120\ \text{cm}^{-3}$ and the latitudinal variation index $\nu = 0.2$ (Figure 4j).

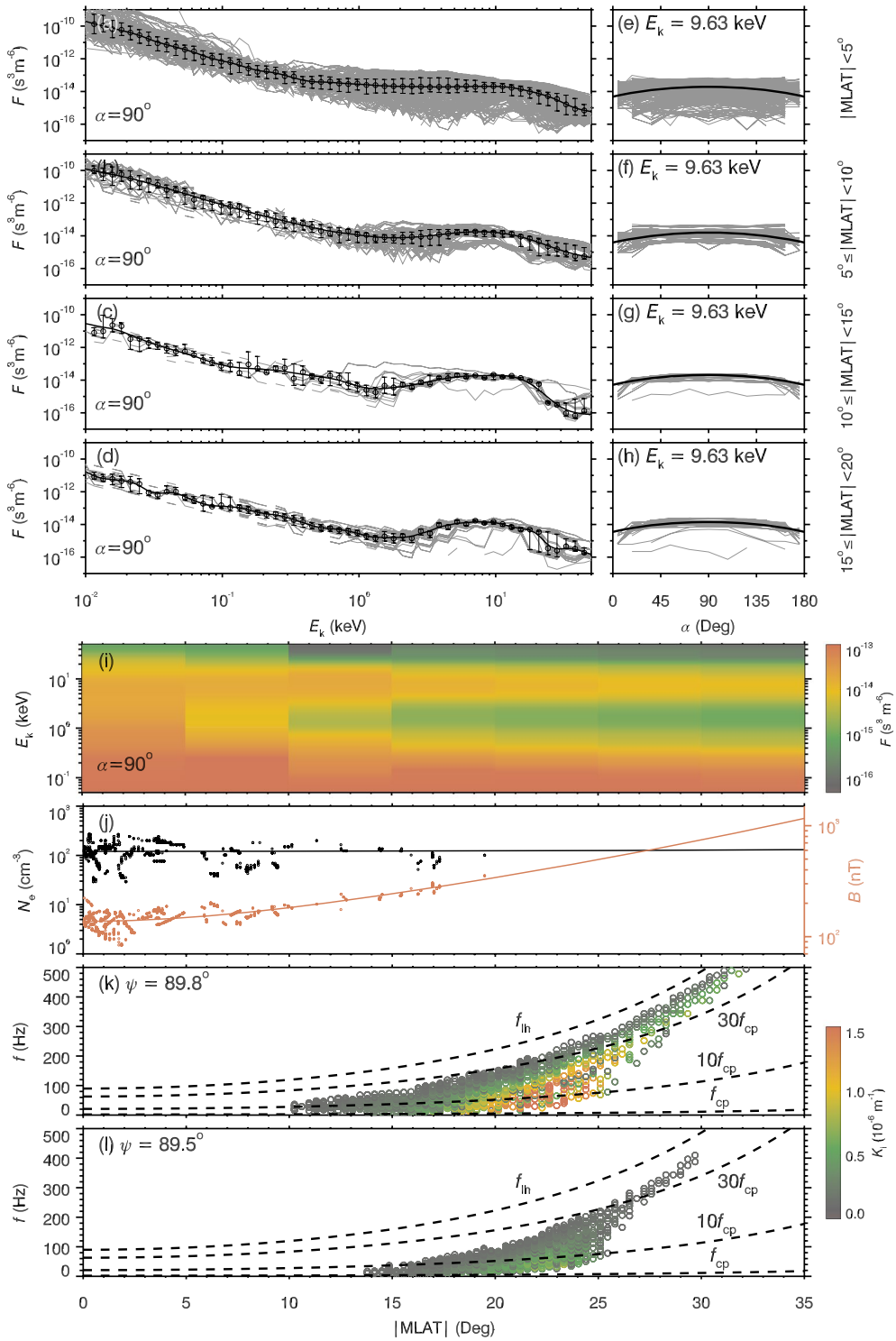

Figure 4. Numerical modeling of the latitude-dependent proton Bernstein-mode instability. (a–d) Proton perpendicular phase space density in the duskside (15 < MLT < 21) outer plasmasphere (5.35 < L < 5.65) for four latitudinal bins (indicated). The gray lines, black circles, and black lines represent the measurements, corresponding median values, and their modeled values, respectively. The vertical error bars indicate the upper and lower quartiles of measurements; (e–h) pitch-angle distribution of proton phase space density of E_k = 9.63 keV in the duskside (15 < MLT <21) outer plasmasphere (5.35 < L < 5.65) for four latitudinal bins (indicated); (i) proton perpendicular phase space density model in the latitude range of 0°–35°; (j) latitude-dependent electron density N_e (black) and magnetic field B (red) measured in the outer plasmasphere 5.35 < L < 5.65 (circles) and modeled analytically (lines); (k and l) latitude-dependent convective growth rate K_i of magnetosonic waves at ψ = 89.8° and ψ = 89.5°.

Figures 4k–4l demonstrate that magnetosonic waves primarily grow at the midlatitudes of 18°–27°. With the local normal angles of $\psi = 89.8°$ and 89.5°, the peak growth rate can reach 1.8×10^{-6} and 3×10^{-7} m^{-1}, respectively. Previous studies (B. Liu et al., 2018; Ma et al., 2014; Posch et al., 2015; Yuan et al., 2018) have suggested that the Alfvén energy is usually too low for magnetosonic wave growth at the equator of the high-density plasmasphere. At the midlatitudes of the plasmasphere, the Alfvén energy could have become appropriate for the proton Bernstein-mode instability. In contrast, outside the plasmasphere, the midlatitude region usually has an overlarge Alfvén energy. As shown in the previous ray-tracing simulations (Wu et al., 2021), these magnetosonic waves could be repeatedly amplified during their bounce-drift propagation near the plasmapause. At latitudes closer to the equator, their normal angles deviate more significantly from 90° (Wu et al., 2021), qualitatively explaining the observations in Figure 3b. Because the Van Allen Probes were located equatorward of the wave source region of 18°–27° most of the time, the measured waves had a median power-weighted wave normal angle $\langle\psi\rangle$ (Figure 3b) below the values selected in the source region (Figures 4k and 4l). The modeled waves with linear growth rates $>5 \times 10^{-7}$ m^{-1} extend up to 300 Hz. When these waves propagate to the equator, the upper frequency limit is approximately $3f_{lh}$, comparable to the observations in Figure 3d. The duskside preference of these $f > f_{lh}$ magnetosonic waves (Figure 2) may be caused by the westward energy-dispersive drift of substorm-injected protons. Previous modeling (Chen et al., 2010) and observations (Kim & Shprits, 2018; Ma et al., 2014; Yuan et al., 2018) have shown that, proton rings prefer to occur inside the plasmasphere on the duskside and outside the plasmasphere on the dayside, and they center at higher energies on the dayside than on the duskside. In the plasmasphere, a proton ring centering at higher energy corresponds to the magnetosonic wave source at higher latitudes, and a longer path from the source to the equator could lead to stronger damping of magnetosonic waves (Horne et al., 2000).

5. Summary

Inspired by recent observations of magnetosonic waves far away from the equator (Boardsen et al., 2016; Ni et al., 2018; Tsurutani et al., 2014; Yuan et al., 2019; Zhima et al., 2015) or above the lower hybrid frequency (Boardsen et al., 2016; Wu et al., 2021), we reexamine the possibility of magnetosonic waves in cyclotron resonance with the radiation belt electrons over a broad range of energies. Our new findings are summarized as follows:

1. The plasmaspheric magnetosonic waves with frequencies $f > f_{lh}$ and normal angles $\psi < 87°$ are in the $n = \pm1$, ±2, and ±3 cyclotron resonances with the radiation belt electrons above 10–100s keV.
2. The $f > f_{lh}$ magnetosonic waves predominantly occur in the duskside ($15 < \text{MLT} < 21$) outer ($5 < L < 6$) plasmasphere. Their amplitude positively correlates with substorm intensity, averaging 10–30 pT following strong substorms. Their upper frequency limit reaches $3.3f_{lh}$, and their normal angles systematically increase from 83.5° at the equator to 85.5° at the farthest latitudes (±20°) sampled by the Van Allen Probes mission.
3. Different from the $f < f_{lh}$ magnetosonic waves generated near the equator, these $f > f_{lh}$ magnetosonic waves are probably generated by the proton Bernstein-mode instability at the midlatitudes of 18°–27° inside the plasmasphere. When these waves propagate toward the equator, their normal angles deviate gradually from 90° and their frequencies could fall above the local lower hybrid frequency.

Although these $f > f_{lh}$ magnetosonic waves are weaker and less common than the $f < f_{lh}$ waves, the variations in wave frequency and normal angle have significantly changed the resonance range of pitch-angles and energies of electrons. Future works may need to quantify the contribution of these $f > f_{lh}$ magnetosonic waves to the radiation belt electron dynamics via cyclotron resonances.

Data Availability Statement

Van Allen Probes data are available at https://spdf.gsfc.nasa.gov/pub/data/rbsp/. Following data are used in this work: EMFISIS L2 WFR Cross Spectral Matrix data (Kletzing & Smith, 2022); EMFISIS L3 Magnetometer data (Kletzing, 2022b) and EMFISIS L4 density data (Kletzing, 2022a); ECT L3 HOPE Ion fluxes data (Funsten, 2022). SME index is available at https://supermag.jhuapl.edu/.

Acknowledgments
The authors acknowledge EMFISIS and ECT teams for the use of Van Allen Probes data and acknowledge the SuperMAG collaborators (http://supermag.jhuapl.edu/info/?page=acknowledgement) for the use of SME index. This work was supported by the Strategic Priority Research Program of Chinese Academy of Sciences (Grant XDB 41000000), the National Natural Science Foundation of China (Grants 42274198, 42188101, 42004140, and 42130204), and the Key Research Program of the Chinese Academy of Sciences (Grant ZDRE-KT-2021-3).

References

Balikhin, M. A., Shprits, Y. Y., Walker, S. N., Chen, L., Cornilleau-Wehrlin, N., Dandouras, I., et al. (2015). Observations of discrete harmonics emerging from equatorial noise. *Nature Communications*, *6*, 7703. https://doi.org/10.1038/ncomms8703

Boardsen, S. A., Gallagher, D. L., Gurnett, D. A., Peterson, W. K., & Green, J. L. (1992). Funnel-shaped, low-frequency equatorial waves. *Journal of Geophysical Research*, *97*, 14967–14976. https://doi.org/10.1029/92JA00827

Boardsen, S. A., Hospodarsky, G. B., Kletzing, C. A., Engebretson, M. J., Pfaff, R. F., Wygant, J. R., et al. (2016). Survey of the frequency dependent latitudinal distribution of the fast magnetosonic wave mode from Van Allen Probes Electric and Magnetic Field Instrument and Integrated Science waveform receiver plasma wave analysis. *Journal of Geophysical Research: Space Physics*, *121*, 2902–2921. https://doi.org/10.1002/2015JA021844

Boardsen, S. A., Hospodarsky, G. B., Min, K., Averkamp, T. F., Bounds, S. R., Kletzing, C. A., & Pfaff, R. F. (2018). Determining the wave vector direction of equatorial fast magnetosonic waves. *Geophysical Research Letters*, *45*(16), 7951–7959. https://doi.org/10.1029/2018GL078695

Bortnik, J., & Thorne, R. M. (2010). Transit time scattering of energetic electrons due to equatorially confined magnetosonic waves. *Journal of Geophysical Research*, *115*, A07213. https://doi.org/10.1029/2010JA015283

Bortnik, J., Thorne, R. M., Ni, B., & Li, J. (2015). Analytical approximation of transit time scattering due to magnetosonic waves. *Geophysical Research Letters*, *42*(5), 1318–1325. https://doi.org/10.1002/2014GL062710

Chen, L. (2015). Wave normal angle and frequency characteristics of magnetosonic wave linear instability. *Geophysical Research Letters*, *42*(12), 4709–4715. https://doi.org/10.1002/2015GL064237

Chen, L., Maldonado, A., Bortnik, J., Thorne, R. M., Li, J., Dai, L., & Zhan, X. (2015). Nonlinear bounce resonances between magnetosonic waves and equatorially mirroring electrons. *Journal of Geophysical Research*, *120*, 6514–6527. https://doi.org/10.1002/2015JA021174

Chen, L., Thorne, R. M., Jordanova, V. K., & Horne, R. B. (2010). Global simulation of magnetosonic wave instability in the storm time magnetosphere. *Journal of Geophysical Research (Space Physics)*, *115*(A11), A11222. https://doi.org/10.1029/2010JA015707

Denton, R. E., Goldstein, J., & Menietti, J. D. (2002). Field line dependence of magnetospheric electron density. *Geophysical Research Letters*, *29*(24), 2205. https://doi.org/10.1029/2002GL015963

Fu, S., Ni, B., Zhou, R., Cao, X., & Gu, X. (2019). Combined scattering of radiation belt electrons caused by Landau and bounce resonant interactions with magnetosonic waves. *Geophysical Research Letters*, *46*(17–18), 10313–10321. https://doi.org/10.1029/2019GL084438

Funsten, H. O. (2022). Van Allen Probe A energetic particle, composition, and thermal plasma suite (ECT) Helium Oxygen Proton Electron, HOPE, mass spectrometer pitch angle resolved science data. Electron fluxes, 15 eV to 50 keV, and ion fluxes, 1 eV to 50 keV, as measured in alternate Spin Cadence, Level 3, Release 4 (L3), 11.35 s Data [Dataset]. NASA Space Physics Data Facility. doi: https://doi.org/10.48322/17p9-rf75

Funsten, H. O., Skoug, R. M., Guthrie, A. A., MacDonald, E. A., Baldonado, J. R., Harper, R. W., et al. (2013). Helium, Oxygen, Proton, and Electron (HOPE) mass spectrometer for the Radiation Belt Storm Probes mission. *Space Science Reviews*, *179*, 423–484. https://doi.org/10.1007/s11214-013-9968-7

Gurnett, D. A. (1976). Plasma wave interactions with energetic ions near the magnetic equator. *Journal of Geophysical Research*, *81*, 2765–2770. https://doi.org/10.1029/JA081i016p02765

Horne, R. B., & Thorne, R. M. (1998). Potential waves for relativistic electron scattering and stochastic acceleration during magnetic storms. *Geophysical Research Letters*, *25*, 3011–3014. https://doi.org/10.1029/98GL01002

Horne, R. B., Thorne, R. M., Glauert, S. A., Meredith, N. P., Pokhotelov, D., & Santolík, O. (2007). Electron acceleration in the Van Allen radiation belts by fast magnetosonic waves. *Geophysical Research Letters*, *34*, L17107. https://doi.org/10.1029/2007GL030267

Horne, R. B., Wheeler, G. V., & Alleyne, H. S. C. K. (2000). Proton and electron heating by radially propagating fast magnetosonic waves. *Journal of Geophysical Research*, *105*, 27597–27610. https://doi.org/10.1029/2000JA000018

Kabin, K., Rankin, R., Mann, I. R., Degeling, A. W., & Marchand, R. (2007). Polarization properties of standing shear Alfvén waves in non-axisymmetric background magnetic fields. *Annales Geophysicae*, *25*(3), 815–822. https://doi.org/10.5194/angeo-25-815-2007

Kim, K.-C., & Shprits, Y. (2018). Survey of the favorable conditions for magnetosonic wave excitation. *Journal of Geophysical Research*, *123*(1), 400–413. https://doi.org/10.1002/2017JA024865

Kletzing, C. A. (2022a). Van Allen Probe A Electric and Magnetic Field Instrument Suite and Integrated Science (EMFISIS) Density and other Parameters derived by digitizing Traces on Spectrograms, Level 4 (L4), 0.5 s Data [Dataset]. NASA Space Physics Data Facility. doi: https://doi.org/10.48322/c4ha-xj50

Kletzing, C. A. (2022b). Van Allen Probe A Fluxgate Magnetometer 1 second resolution data in GSM coordinates. [Dataset]. NASA Space Physics Data Facility. https://doi.org/10.48322/w6r4-fp76

Kletzing, C. A., & Smith, C. W. (2022). Van Allen Probe A Electric and Magnetic Field Instrument Suite and Integrated Science (EMFISIS) Waveform Receiver (WFR) Cross Spectral Matrix, Level 2 (L2), 6 s Data [Dataset]. NASA Space Physics Data Facility. doi: https://doi.org/10.48322/be1v-n754

Kletzing, C. A., Kurth, W. S., Acuna, M., MacDowall, R. J., Torbert, R. B., Averkamp, T., et al. (2013). The electric and magnetic field instrument suite and integrated science (EMFISIS) on RBSP. *Space Science Reviews*, *179*, 127–181. https://doi.org/10.1007/s11214-013-9993-6

Kurth, W. S., De Pascuale, S., Faden, J. B., Kletzing, C. A., Hospodarsky, G. B., Thaller, S., & Wygant, J. R. (2015). Electron densities inferred from plasma wave spectra obtained by the Waves instrument on Van Allen Probes. *Journal of Geophysical Research (Space Physics)*, *120*(2), 904–914. https://doi.org/10.1002/2014JA020857

Li, J., Ni, B., Ma, Q., Xie, L., Pu, Z., Fu, S., et al. (2016). Formation of energetic electron butterfly distributions by magnetosonic waves via Landau resonance. *Geophysical Research Letters*, *43*, 3009–3016. https://doi.org/10.1002/2016GL067853

Li, J., Ni, B., Xie, L., Pu, Z., Bortnik, J., Thorne, R. M., et al. (2014). Interactions between magnetosonic waves and radiation belt electrons: Comparisons of quasi-linear calculations with test particle simulations. *Geophysical Research Letters*, *41*, 4828–4834. https://doi.org/10.1002/2014GL060461

Li, L. Y., Yu, J., Cao, J. B., Yang, J. Y., Li, X., Baker, D. N., et al. (2017). Roles of whistler mode waves and magnetosonic waves in changing the outer radiation belt and the slot region. *Journal of Geophysical Research (Space Physics)*, *122*(5), 5431–5448. https://doi.org/10.1002/2016JA023634

Li, W., Thorne, R. M., Bortnik, J., Nishimura, Y., Angelopoulos, V., Chen, L., et al. (2010). Global distributions of suprathermal electrons observed on THEMIS and potential mechanisms for access into the plasmasphere. *Journal of Geophysical Research*, *115*, A00J10. https://doi.org/10.1029/2010JA015687

Liu, B., Li, L., Yu, J., & Cao, J. (2018). The effect of hot protons on magnetosonic waves inside and outside the plasmapause: New observations and theoretic results. *Journal of Geophysical Research (Space Physics)*, *123*(1), 653–664. https://doi.org/10.1002/2017JA024676

Liu, N., Su, Z., Zheng, H., Wang, Y., & Wang, S. (2018a). Magnetosonic harmonic falling and rising frequency emissions potentially generated by nonlinear wave-wave interactions in the Van Allen Radiation Belts. *Geophysical Research Letters*, *45*(16), 7985–7995. https://doi.org/10.1029/2018GL079232

Liu, N., Su, Z., Zheng, H., Wang, Y., & Wang, S. (2018b). Prompt disappearance and emergence of radiation belt magnetosonic waves induced by solar wind dynamic pressure variations. *Geophysical Research Letters*, *45*(2), 585–594. https://doi.org/10.1002/2017GL076382

Maldonado, A. A., & Chen, L. (2018). On the diffusion rates of electron bounce resonant scattering by magnetosonic waves. *Geophysical Research Letters*, *45*(8), 3328–3337. https://doi.org/10.1002/2017GL076560

Ma, Q., Li, W., Bortnik, J., Kletzing, C. A., Kurth, W. S., Hospodarsky, G. B., & Wygant, J. R. (2019). Global survey and empirical model of fast magnetosonic waves over their full frequency range in Earth's inner magnetosphere. *Journal of Geophysical Research (Space Physics)*, *124*(12), 10270–10282. https://doi.org/10.1029/2019JA027407

Ma, Q., Li, W., Chen, L., Thorne, R. M., & Angelopoulos, V. (2014). Magnetosonic wave excitation by ion ring distributions in the Earth's inner magnetosphere. *Journal of Geophysical Research (Space Physics)*, *119*(2), 844–852. https://doi.org/10.1002/2013JA019591

Ma, Q., Li, W., Thorne, R. M., & Angelopoulos, V. (2013). Global distribution of equatorial magnetosonic waves observed by THEMIS. *Geophysical Research Letters*, *40*, 1895–1901. https://doi.org/10.1002/grl.50434

Mauk, B. H., Fox, N. J., Kanekal, S. G., Kessel, R. L., Sibeck, D. G., & Ukhorskiy, A. (2013). Science objectives and rationale for the Radiation Belt Storm Probes Mission. *Space Science Reviews*, *179*, 3–27. https://doi.org/10.1007/s11214-012-9908-y

Meredith, N. P., Horne, R. B., & Anderson, R. R. (2008). Survey of magnetosonic waves and proton ring distributions in the Earth's inner magnetosphere. *Journal of Geophysical Research*, *113*, A06213. https://doi.org/10.1029/2007JA012975

Moldwin, M. B., Thomsen, M. F., Bame, S. J., McComas, D. J., & Moore, K. R. (1994). An examination of the structure and dynamics of the outer plasmasphere using multiple geosynchronous satellites. *Journal of Geophysical Research*, *99*(A6), 11475–11482. https://doi.org/10.1029/93JA03526

Němec, F., Santolík, O., Pickett, J. S., Hrbáčková, Z., & Cornilleau-Wehrlin, N. (2013). Azimuthal directions of equatorial noise propagation determined using 10 years of data from the Cluster spacecraft. *Journal of Geophysical Research (Space Physics)*, *118*(11), 7160–7169. https://doi.org/10.1002/2013JA019373

Newell, P. T., & Gjerloev, J. W. (2011). Evaluation of SuperMAG auroral electrojet indices as indicators of substorms and auroral power. *Journal of Geophysical Research (Space Physics)*, *116*(A12), A12211. https://doi.org/10.1029/2011JA016779

Ni, B., Zou, Z., Fu, S., Cao, X., Gu, X., & Xiang, Z. (2018). Resonant scattering of radiation belt electrons by off-equatorial magnetosonic waves. *Geophysical Research Letters*, *45*(3), 1228–1236. https://doi.org/10.1002/2017GL075788

Posch, J. L., Engebretson, M. J., Olson, C. N., Thaller, S. A., Breneman, A. W., Wygant, J. R., et al. (2015). Low-harmonic magnetosonic waves observed by the Van Allen Probes. *Journal of Geophysical Research (Space Physics)*, *120*(8), 6230–6257. https://doi.org/10.1002/2015JA021179

Russell, C. T., Holzer, R. E., & Smith, E. J. (1970). OGO 3 observations of ELF noise in the magnetosphere. 2. The nature of the equatorial noise. *Journal of Geophysical Research*, *75*, 755–768. https://doi.org/10.1029/JA075i004p00755

Santolík, O., Nemec, F., Gereová, K., Macúšová, E., Conchy, Y., & Cornilleau-Wehrlin, N. (2004). Systematic analysis of equatorial noise below the lower hybrid frequency. *Annales Geophysicae*, *22*(7), 2587–2595. https://doi.org/10.5194/angeo-22-2587-2004

Santolík, O., Parrot, M., & Lefeuvre, F. (2003). Singular value decomposition methods for wave propagation analysis. *Radio Science*, *38*, 1010. https://doi.org/10.1029/2000RS002523

Sheeley, B. W., Moldwin, M. B., Rassoul, H. K., & Anderson, R. R. (2001). An empirical plasmasphere and trough density model: CRRES observations. *Journal of Geophysical Research*, *106*, 25631–25642. https://doi.org/10.1029/2000JA000286

Shprits, Y. Y. (2016). Estimation of bounce resonant scattering by fast magnetosonic waves. *Geophysical Research Letters*, *43*(3), 998–1006. https://doi.org/10.1002/2015GL066796

Spence, H. E., Reeves, G. D., Baker, D. N., Blake, J. B., Bolton, M., Bourdarie, S., et al. (2013). Science goals and overview of the Radiation Belt Storm Probes (RBSP) energetic particle, composition, and thermal plasma (ECT) suite on NASA's Van Allen Probes Mission. *Space Science Reviews*, *179*(1–4), 311–336. https://doi.org/10.1007/s11214-013-0007-5

Stix, T. H. (1962). *The theory of plasma waves*. McGraw-Hill.

Su, Z., Liu, N., Zheng, H., Wang, Y., & Wang, S. (2018). Large-amplitude extremely low frequency hiss waves in plasmaspheric plumes. *Geophysical Research Letters*, *45*(2), 565–577. https://doi.org/10.1002/2017GL076754

Su, Z., Wang, G., Liu, N., Zheng, H., Wang, Y., & Wang, S. (2017). Direct observation of generation and propagation of magnetosonic waves following substorm injection. *Geophysical Research Letters*, *44*(15), 7587–7597. https://doi.org/10.1002/2017GL074362

Summers, D., Ni, B., & Meredith, N. P. (2007). Timescales for radiation belt electron acceleration and loss due to resonant wave-particle interactions: 1. Theory. *Journal of Geophysical Research (Space Physics)*, *112*(A4), A04206. https://doi.org/10.1029/2006JA011801

Summers, D., Thorne, R. M., & Xiao, F. (1998). Relativistic theory of wave-particle resonant diffusion with application to electron acceleration in the magnetosphere. *Journal of Geophysical Research*, *103*, 20487. https://doi.org/10.1029/98JA01740

Tao, X., & Li, X. (2016). Theoretical bounce resonance diffusion coefficient for waves generated near the equatorial plane. *Geophysical Research Letters*, *43*(14), 7389–7397. https://doi.org/10.1002/2016GL070139

Teng, S., Li, W., Tao, X., Ma, Q., & Shen, X. (2019). Characteristics and generation of low-frequency magnetosonic waves below the proton gyrofrequency. *Geophysical Research Letters*, *46*(21), 11652–11660. https://doi.org/10.1029/2019GL085372

Tsurutani, B. T., Falkowski, B. J., Pickett, J. S., Verkhoglyadova, O. P., Santolik, O., & Lakhina, G. S. (2014). Extremely intense ELF magnetosonic waves: A survey of polar observations. *Journal of Geophysical Research*, *119*, 964–977. https://doi.org/10.1002/2013JA019284

Wu, Z., Su, Z., Liu, N., Gao, Z., Zheng, H., Wang, Y., & Wang, S. (2021). Off-equatorial source of magnetosonic waves extending above the lower hybrid resonance frequency in the inner magnetosphere. *Geophysical Research Letters*, *48*(6), e2020GL091830. https://doi.org/10.1029/2020GL091830

Xiao, F., Yang, C., Su, Z., Zhou, Q., He, Z., He, Y., et al. (2015). Wave-driven butterfly distribution of Van Allen belt relativistic electrons. *Nature Communications*, *6*, 8590. https://doi.org/10.1038/ncomms9590

Yan, L., Cao, X., Hua, M., Ni, B., & Zhang, Y. (2021). Statistics of magnetosonic waves in the slot region observed by Van Allen Probes. *Geophysical Research Letters*, *48*(14), e94015. https://doi.org/10.1029/2021GL094015

Yu, J., Li, L. Y., Cui, J., Cao, J. B., & Wang, J. (2019). Effect of low-harmonic magnetosonic waves on the radiation belt electrons inside the plasmasphere. *Journal of Geophysical Research (Space Physics)*, *124*(5), 3390–3401. https://doi.org/10.1029/2018JA026328

Yu, X., Yuan, Z., Yao, F., Ouyang, Z., & Wang, D. (2021). Electromagnetic characteristics of fast magnetosonic waves in the inner magnetosphere. *Journal of Geophysical Research (Space Physics)*, *126*(9), e29759. https://doi.org/10.1029/2021JA029759

Yu, X., Yuan, Z., & Yu, J. (2020). Revisit the analytical approximation of transit-time scattering for fast magnetosonic waves. *Geophysical Research Letters*, *47*(16), e88434. https://doi.org/10.1029/2020GL088434

Yuan, Z., Ouyang, Z., Yu, X., Huang, S., Yao, F., & Funsten, H. O. (2018). Global distribution of proton rings and associated magnetosonic wave instability in the inner magnetosphere. *Geophysical Research Letters*, *45*(19), 10160–10166. https://doi.org/10.1029/2018GL079999

Yuan, Z., Yao, F., Yu, X., Huang, S., & Ouyang, Z. (2019). An automatic detection algorithm applied to fast magnetosonic waves with observations of the Van Allen Probes. *Journal of Geophysical Research (Space Physics)*, *124*(5), 3501–3511. https://doi.org/10.1029/2018JA026387

Zhima, Z., Chen, L., Fu, H., Cao, J., Horne, R. B., & Reeves, G. (2015). Observations of discrete magnetosonic waves off the magnetic equator. *Geophysical Research Letters*, *42*(22), 9694–9701. https://doi.org/10.1002/2015GL066255